ELSEVIER

International Journal of Pharmaceutics 246 (2002) 61–73

international journal of pharmaceutics

www.elsevier.com/locate/ijpharm

Use of commercial porous ceramic particles for sustained drug delivery

R.S. Byrne *, P.B. Deasy

Department of Pharmaceutics and Pharmaceutical Technology, School of Pharmacy, University of Dublin, Trinity College, Dublin 2, Ireland

Received 1 May 2002; received in revised form 27 June 2002; accepted 28 June 2002

Abstract

Three commercially available microparticulate porous ceramics, N-light N3, Starlight SLK1000 and Carbolite 16/20, were characterised using a range of techniques. Starlight SLK1000 and Carbolite 16/20 were principally composed of mullite, while N-light N3 was principally composed of quartz. Each porous ceramic was partly open-cell with varying porosities and pore size distributions. Using a novel vacuum loading technique, N-light N3 was loaded with benzoic acid, sodium benzoate and diltiazem HCl, while Starlight SLK1000 and Carbolite 16/20 were loaded with diltiazem HCl. The drug loading was influenced by the solution concentration and by the porosity and bulk density of the ceramic. In vitro dissolution testing of the loaded porous microparticles showed an initial burst release of each drug followed by sustained release. The release was influenced by the surface pore size distribution of the ceramic and by electrostatic interactions between the interior and exterior microparticle surfaces and the drug.

Keywords: Diltiazem HCl; Floating; Microparticles; Porous ceramics; Sustained release; Vacuum loading

1. Introduction

Porous ceramics are bodies comprised of a three-dimensional array of hollow polygons, known as cells. If the individual cells are interconnected the porous ceramic is termed open-cell, while if they are isolated from each other, the porous ceramic is termed closed-cell. They can also be partly open or partly closed. Porous ceramics have been produced from many materials such as cordierite, mullite, silicon carbide and alumina, and by various processing routes such as capsule-free hot isostatic pressing, gelcasting and the polymeric sponge method (Montanaro et al., 1998). Both the properties of the ceramic powder and the processing method used greatly influence the extent of porosity, the pore morphology and pore size distribution of the final material (Ishizaki et al., 1998).

In recent years there has been increasing interest in such materials. They have found many applications including catalyst supports, filters for molten metals and hot gases, refractory linings for fur-

* Corresponding author. Tel.: +353-1-6082836; fax: +353-1-6082783

E-mail address: byrners@tcd.ie (R.S. Byrne).

0378-5173/02/$ - see front matter
PII: S0378-5173(02)00357-5

naces, and porous implants in the area of biomaterials (Sepulveda and Binner, 1999). Porous ceramics have also found uses in drug delivery, with calcium phosphate ceramics being investigated principally. The majority of this work has been done on implantable blocks or cylinders. Drugs such as cisplatin (Netz et al., 2001), hydrocortisone acetate (Krajewski et al., 2000), isepamicin sulfate (Itokazu et al., 1998), methotrexate (Itokazu et al., 1999) and 5-flurouracil (Landi et al., 2000) have been loaded into these implantable blocks or cylinders. Some work has also been carried out on calcium phosphate granules and pellets loaded with sodium ampicillin (Queiroz et al., 2001) and gentamicin (Thoma and Alex, 1991), respectively. An alumina porous ceramic loaded with hydrocortisone acetate (Krajewski et al., 2000) has also been investigated. Collectively this work has demonstrated the potential of porous ceramics as drug delivery systems, which provide sustained release.

This research paper focuses on potential applications of non-calcium phosphate commercially produced microparticulate porous ceramics in sustained drug delivery with a view to developing applications in oral drug delivery and also in sustained chemical delivery. Three different microparticulate porous ceramics were obtained from commercial suppliers. Two of these, N-light N3 and Starlight SLK1000, are marketed for use in the building industry. For example, they can be used as aggregates for light concrete and mortar to produce heat resistant blocks. The third porous ceramic examined, Carbolite 16/20, is marketed for use in the hydraulic fracturing of oil and gas wells.

2. Materials and methods

2.1. Materials

Benzoic acid, sodium benzoate, sodium hydroxide (Sigma), Carbolite 16/20 (Carboceramics, USA), diltiazem HCl (Seloc PCAS, France), disodium hydrogen phosphate dodecahydrate, sodium dihydrogen phosphate dihydrate (Merck), ethanol (Cooley Distillery, Ireland), hydrochloric acid, potassium chloride (BDH), N-light N3 (Itochu Ceratech Corporation, Japan), Starlight SLK 1000 (Imerys, UK) and water (HPLC grade and deionised) were used.

2.2. Sieve analysis of porous ceramic microparticles

Sieve analysis on random samples of each porous ceramic was performed using a nest of standard sieves, 1400, 1180, 1000, 850, 710, 600 and 500 μm, agitated for 10 min on a sieve shaker (Endecott) and the retained weight data obtained was used to construct a frequency distribution. The size range 850–1000 μm was selected for use in further experiments.

2.3. Scanning electron microscopy and energy dispersive X-ray microanalysis of porous ceramic microparticles

Samples of porous ceramic microparticles were mounted on aluminium stubs using double-sided sticky tape, vacuum coated with gold in a sputter coater (Polaron SC500) and examined using a field emission scanning electron microscope (SEM) (Hitachi S4300). Cross-sections of N-light N3 and Starlight SLK1000 were mounted and examined in a similar manner. Cross-sections of Carbolite 16/20 were prepared by embedding the microparticles in an epoxy resin and grinding to give a flat polished surface. This surface was then vacuum coated with gold and examined.

Qualitative energy dispersive X-ray (EDX) microanalysis was carried out using a variable pressure SEM (Hitachi S-3500N) and an X-ray detector (Princeton Gamma Tech). To examine microparticle surfaces or cross-sections, they were mounted on aluminium stubs using adhesive carbon tabs. To examine Carbolite 16/20 cross-sections, the epoxy resin embedded surface was coated in carbon.

2.4. X-Ray diffraction of porous ceramic microparticles

X-ray diffraction (XRD) patterns of crushed samples of the porous ceramic microparticles were obtained using a Siemens D500 X-ray powder diffractometer. A 1.0° dispersion slit, a 1.0° anti-

scatter slit, and a 0.15° receiving slit were used. Powdered samples of each porous ceramic were studied by placing a thin layer of the powder in conventional cavity mounts. Measurements were taken from 10.000 to 90.000° on the 2θ scale at a step size of 0.020°/s. The Cu anode X-ray was operated at 40 kV and 30 mA in combination with a Ni filter to give monochromatic Cu Kα X-rays.

2.5. Zeta potential of porous ceramic microparticles

A 0.001 M potassium chloride solution containing 0.1 mg of crushed porous ceramic per ml was prepared using HPLC grade deionised water. Using aliquots of this suspension, a series of suspensions with a range of pHs were prepared. The pH was adjusted using hydrochloric acid and sodium hydroxide solutions. The zeta potential of each suspension was measured using a calibrated Zetasizer 3000 (Malvern).

2.6. Mercury porosimetry and helium pycnometry studies on porous ceramic microparticles

For both mercury porosimetry and helium pycnometry, the samples were dried overnight to a constant weight in a vacuum oven at 50 °C with a vacuum pressure of 600 mbar. Mercury porosimetry was performed using a Poresizer 9320 (Micromeritics). A calibrated 5 cm^3 'solid sample' penetrometer was used. A mass of sample sufficient to almost fill the penetrometer bulb was accurately weighed. A manual low-pressure analysis (0.5 to $\sim$20 psi) with automatic reporting was performed, followed by an automatic high-pressure analysis ($\sim$20 to 30 000 psi). The automatic high-pressure analysis was conducted allowing for a 10 s equilibration time.

Helium pycnometry was carried out using an AccuPyc 1330 (Micromeritics) with a 1 cm^3 sample cup. Both whole and crushed porous ceramic samples were analysed, with their mass being accurately determined following analysis. The pycnometer used 10 purges at 19.5 psi and five analytical runs at 19.5 psi with an equilibration rate of 0.0050 psi/min. For both helium pycnometry and mercury porosimetry each sample was analysed in duplicate.

2.7. Surface area analysis of porous ceramic microparticles

Surface area analysis was carried out using the Gemini II 2370 Surface Area Analyser (Micromeritics). The saturation pressure of nitrogen was determined at the beginning of each day. The samples to be analysed were degassed for 2 h at 200 °C using the Flow Prep 060 Degasser (Micromeritics).

2.8. Drug loading of porous ceramic microparticles

Three methods were investigated for loading N-light N3 with diltiazem HCl. Each method was carried out in triplicate and crushed samples of the resulting drug loaded porous ceramics were assayed for drug content by UV spectroscopy (Spectronic Genesye 5). Based on these results, a method was selected for other loading experiments.

Method (i): Three grams of N-light N3 microparticles were placed in 33 ml of a 40% w/v diltiazem HCl solution and stirred for 30 min using a magnetic stirrer. The microparticles and drug solution were then allowed to stand for 1 h. Following this, they were separated using filter paper and dried for 24 h at 60 °C.

Method (ii): Three grams of N-light N3 microparticles were placed in 33 ml of a 40% w/v diltiazem HCl solution. The mixture was evacuated for 30 min after which the vacuum was released. The microparticles and drug solution were then allowed to stand for 1 h. Following this, they were separated using filter paper and dried for 24 h at 60 °C.

Method (iii): Three grams of N-light N3 microparticles were placed in a 10 ml specimen tube, which was capped with a lid containing a single 1 mm hole. The tube was placed in a 50 ml round bottomed flask with the lid to the bottom. A stopcock was attached to the flask. With the stopcock open, the flask was evacuated for 30 min (Fig. 1(a)). Thirty-three millilitre of a 40% w/v diltiazem HCl solution was introduced to the flask

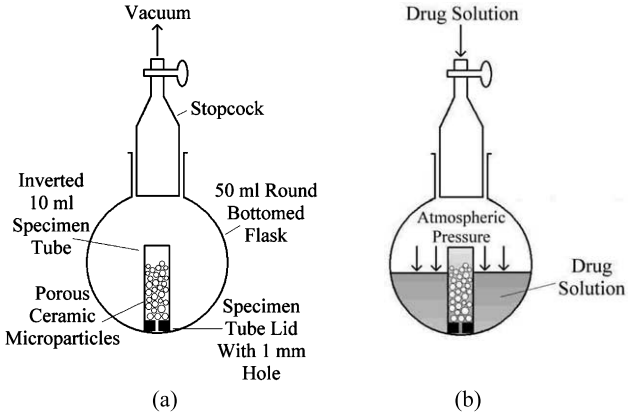

Fig. 1. Representation of drug loading method (iii), (a) prior to introduction of drug solution and (b) following introduction of drug solution and restoration of atmospheric pressure.

through the stopcock. The microparticles and drug solution were allowed to stand for 1 h (Fig. 1(b)). Following this, they were separated using filter paper and dried for 24 h at 60 °C.

Using method (iii), 3 g of N-light N3 microparticles were also loaded using a 40% w/v aqueous sodium benzoate solution and a 30% w/v ethanolic benzoic acid solution. 1.5 g of Starlight SLK1000 and 9.39 g of Carbolite 16/20 were loaded with a 40% w/v diltiazem HCl solution.

2.9. Dissolution testing of drug loaded porous ceramic microparticles

Each drug loaded porous ceramic was subjected to dissolution testing at 37 °C for 24 h in 900 ml of phosphate buffer pH 6.8 using an EP dissolution basket assembly rotating at 100 rpm, located 25 mm above the base of the vessel (Erweka DT6). Adequate sink conditions existed. Five millilitre samples were withdrawn periodically with immediate replacement of the dissolution medium, and following filtration through a 0.45 μm filter (Gelman), were assayed by UV spectroscopy. The repeated removal of sample from the dissolution medium was accounted for in the subsequent calculations. Dissolution tests were carried out in triplicate.

Following dissolution testing, the sample was crushed and assayed for drug content. The average percentage release was found based on the release at 24 h and the drug remaining in the microparticles following dissolution testing. Dissolution testing was also carried out on certain crushed drug loaded porous ceramic samples.

2.10. Analysis of variance

The statistical technique ANOVA was used to compare sample means. The difference between sample means was deemed statistically significant if the 95% confidence intervals for the means did not overlap.

3. Results and discussion

3.1. Sieve analysis of porous ceramic microparticles

The results of sieve analysis of the porous ceramic microparticles are shown in Fig. 2. It can be seen that Carbolite 16/20 had the narrowest size distribution with 71.0% w/w of microparticles in the size range 1000–1180 μm. 30.7% w/w of N-light N3 microparticles were in the size range 710–850 μm, while 38.1% w/w of Starlight SLK1000 microparticles were less than 500 μm in diameter. This fraction contained a high level of fines, which was attributed to crushing of the Starlight SLK1000 microparticles during storage, as they were relatively brittle. In the 850–1000 μm size

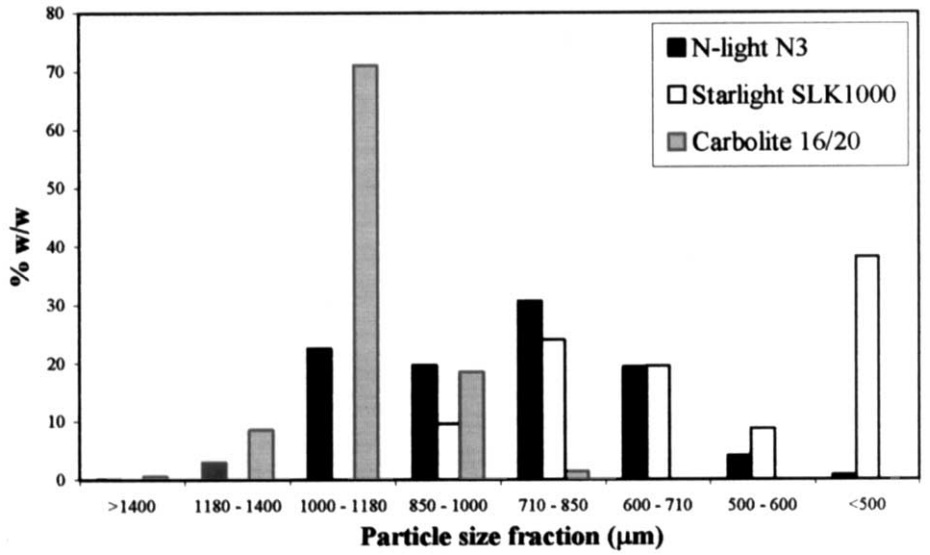

Fig. 2. Particle size distribution of N-light N3, Starlight SLK1000 and Carbolite 16/20.

fraction there was at least 9.5% w/w of the microparticles for each porous ceramic. For this reason this size fraction was used in all further comparative experiments.

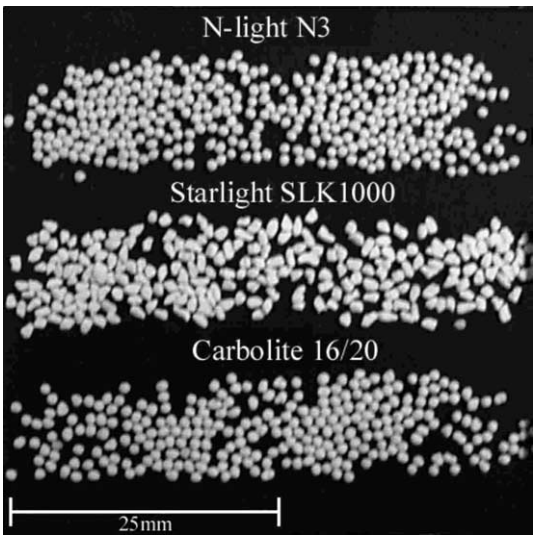

Fig. 3. Photograph of N-light N3, Starlight SLK1000 and Carbolite 16/20 microparticles.

3.2. Appearance of the porous ceramic microparticles

The general appearance of the microparticles is shown in Fig. 3. Both N-light N3 and Carbolite 16/20 were spherical, while Starlight SLK1000 consisted of microparticles of a variety of shapes. In the electron micrographs of the surface of each material, shown in Fig. 4(a–c), surface pores were evident. Each porous ceramic differed in the surface pore sizes with the largest being observed in Starlight SLK1000.

Electron micrographs of cross-sections of the microparticles are shown in Fig. 4(d–f). While the porous structure of Starlight SLK1000 and Carbolite 16/20 seen in surface view is apparent in cross-section, that of N-light N3 is quite different. Larger pores, up to 400 μm in diameter, can be seen in Fig. 4(d).

The electron micrographs suggest both N-light N3 and Starlight SLK1000 have high porosity relative to Carbolite 16/20. The variations in porous structure indicate differing manufacturing techniques have been used in their production.

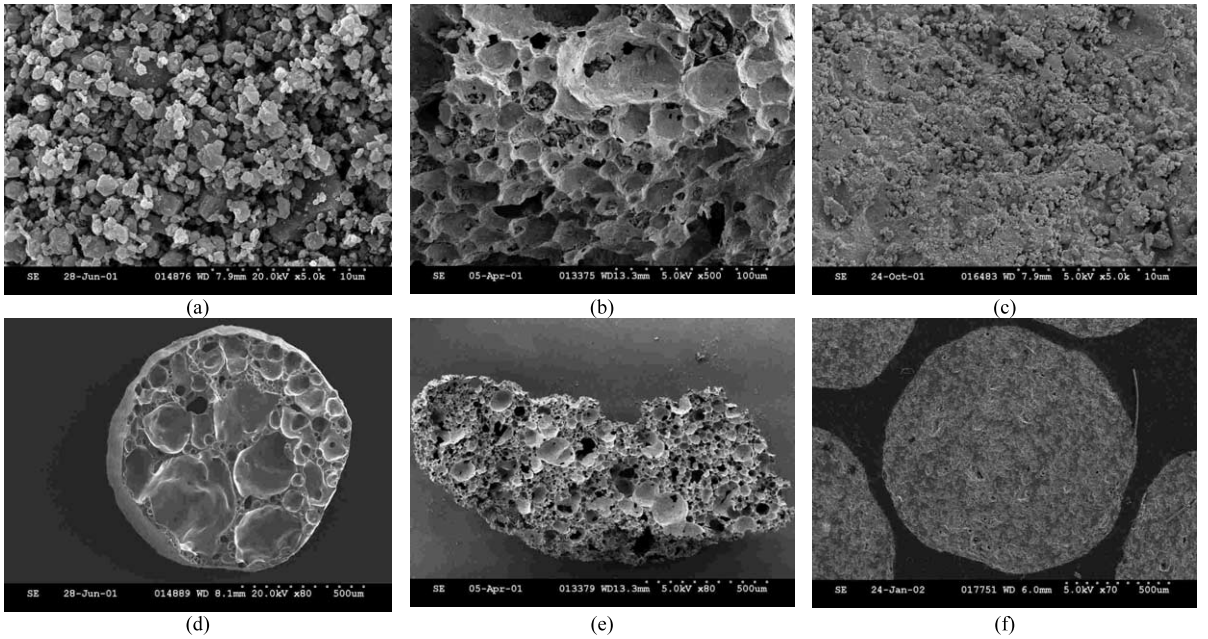

Fig. 4. SEM micrographs of the surface of (a) an N-light N3 microparticle (magnification $\times 5000$) (b) a Starlight SLK1000 microparticle (magnification $\times 500$) (c) a Carbolite 16/20 microparticle (magnification $\times 5000$) and SEM micrographs of cross-sections of (d) an N-light N3 microparticle (magnification $\times 80$) (e) a Starlight SLK1000 microparticle (magnification $\times 80$) and (f) a Carbolite 16/20 microparticle (magnification $\times 70$).

3.3. Elemental and ceramic composition of the porous microparticles

Using EDX microanalysis, it was found that each porous ceramic was principally composed of aluminium and silica with smaller amounts of other elements present. N-light N3 also contained iron and potassium, while Carbolite 16/20 contained iron and titanium. Starlight SLK1000 contained low levels of potassium, titanium and iron.

Fig. 5 shows the XRD patterns of powdered samples of each porous ceramic microparticle. The patterns indicated that N-light N3 was composed of α quartz and feldspar, Starlight SLK1000 of mullite and α quartz, and Carbolite 16/20 of mullite and cristobalite. These XRD results confirm information found in material safety data sheets for the porous ceramic microparticles.

3.4. Zeta potential of porous ceramic microparticles

From Fig. 6 it can be seen that each porous ceramic material had similar zeta potentials over a range of pHs, with Starlight SLK1000 having slightly lower zeta potentials over the complete pH range examined than N-light N3 and Carbolite 16/20. For each porous ceramic there was a rapid fall in zeta potential at low pHs followed by a slowing in this rate. All porous ceramics had a negative zeta potential above pH 4 indicating good potential to bind cationic drugs like diltiazem HCl.

3.5. Mercury porosimetry, helium pycnometry and surface area analysis studies on porous ceramic microparticles

Mercury porosimetry was used to provide information on the bulk density and porous

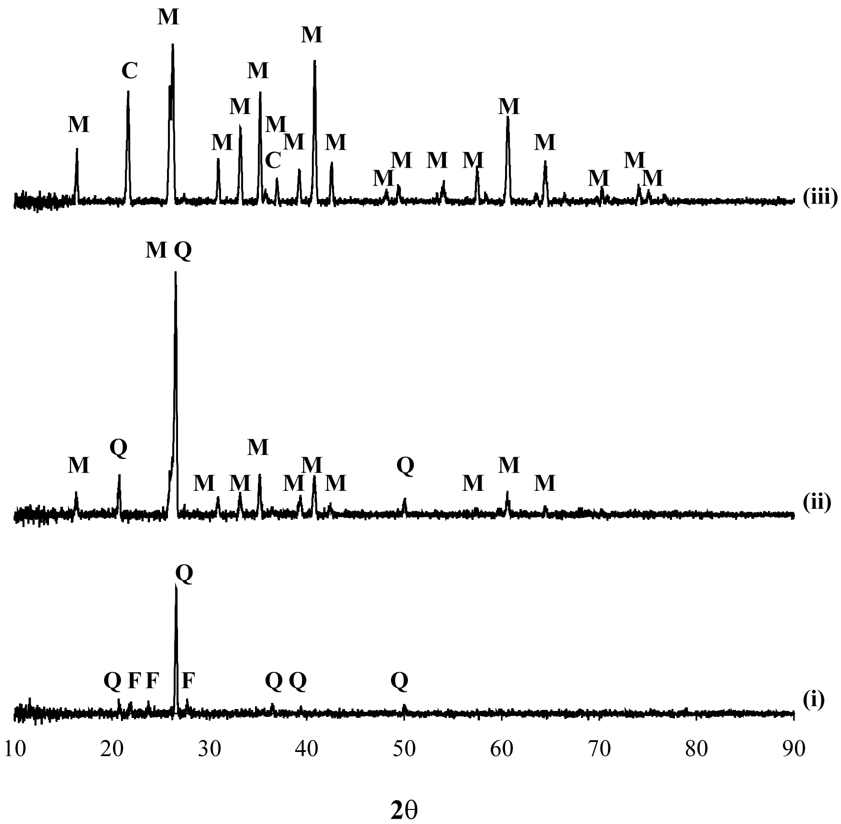

Fig. 5. XRD patterns of crushed samples of: (i) N-light N3; (ii) Starlight SLK1000; (iii) Carbolite 16/20 (C, cristobalite; F, feldspar; M, mullite; Q, α quartz).

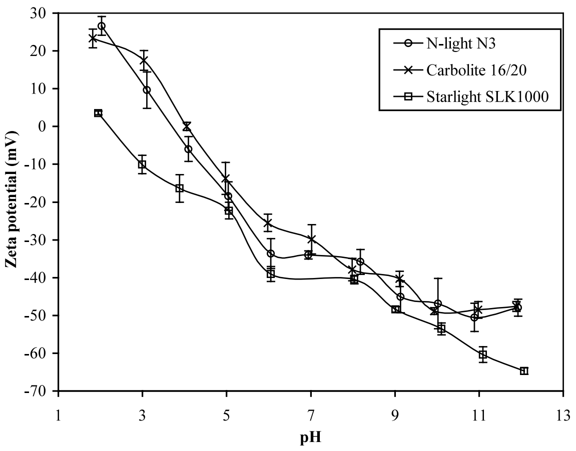

Fig. 6. Zeta potential of N-light N3, Starlight SLK1000 and Carbolite 16/20 over a range of pHs.

microstructure of the porous ceramics. Both N-light N3 and Starlight SLK1000 had bulk densities less than water, while that of Carbolite 16/20 was greater than water (Table 1). This should be of benefit in sustained drug delivery as it has been found that both floating dosage forms and dosage forms with high densities gave increased transit time through the gastrointestinal tract (GIT) (Bechgaard and Ladefoged, 1978; Kawashima et al., 1991). Using cumulative mercury intrusion data, a D_{90} value i.e. the pore diameter below which 90% of the cumulative intrusion occurs, was calculated. For Starlight SLK1000 this was 69.97 µm. The lowest pore diameters measured were 0.1 µm. The D_{90} value for N-light N3 and Carbolite 16/20 was 0.38 and 0.13 µm, respectively. The lowest pore diameter measured for N-light N3 was 0.006 µm (the lower limit of detection of the mercury poresizer), while for Carbolite 16/20 it

Table 1
Densities, porosities and surface areas of N-light N3, Starlight SLK1000 and Carbolite 16/20

Porous ceramic	Bulk density		Skeletal density		Open porosity		Closed porosity		Total porosity		BET multipoint surface area	
	Average (g/ml)	S.D.	Average (g/ml)	S.D.	Average (% v/v)	S.D.	Average (% v/v)	S.D.	Average (% v/v)	S.D.	Average (m^2/g)	S.D.
N-light N3	0.7312	0.0046	1.4095	0.0055	48.36	0.36	21.34	0.56	69.70	0.44	0.6606	0.0142
Starlight SLK1000	0.3665	0.0072	1.6873	0.0239	78.92	1.69	6.99	2.40	85.91	1.70	1.7513	0.1111
Carbolite 16/20	2.5060	0.0059	2.8044	0.0029	10.64	0.03	0.92	0.04	11.56	0.03	0.6449	0.0304

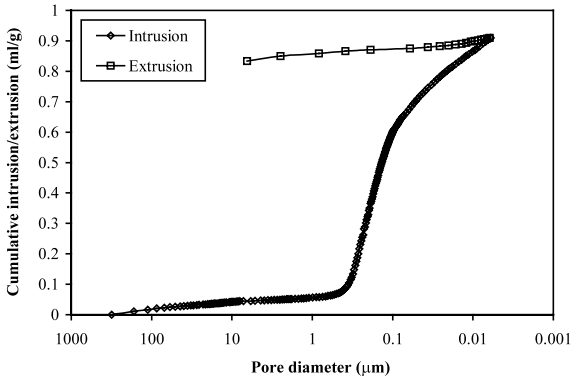

Fig. 7. Cumulative mercury intrusion and extrusion curves versus pore diameter for N-light N3.

was 0.0279 μm. For each porous ceramic a hysteresis between the cumulative mercury intrusion and extrusion curves was seen. This is shown for N-light N3 in Fig. 7. Hysteresis are usually seen when mercury has been trapped in pores with a narrow neck leading to a large pore interior (Moscou and Lub, 1981). In this case the hysteresis is due to smaller surface pores connecting to larger interior pores.

As discussed above, large N-light N3 interior pores were seen in SEM, which were not evident in surface view. Their pore sizes were not measured by mercury porosimetry as in order for mercury to intrude these pores it had to connect through the narrow surface pores. Therefore, the larger interior pores were measured as though their diameters were those of the surface pores. Similarly, the small pores detected in Starlight SLK1000 were due to mercury passing through cracks in the surface pores, as seen in Fig. 4(b), in order to reach the interior pores. SEM observations found these cracks typically had diameters less than 10 μm.

Table 1 gives details of the porosities of each ceramic. These values were calculated using bulk and skeletal densities of uncrushed porous ceramic and the skeletal density of crushed porous ceramic. A wide variation in the porosity values was seen. Each porous ceramic had both open and closed pores and therefore the porous ceramics may be described as partly open-cell. The open porosities of the ceramics were reflected in their BET multipoint surface areas. The surface area per microparticle was markedly higher than that of a non-porous sphere of the same average diameter. A linear correlation between the surface area and porosity values was not observed. This was due to the differences in the pore size distributions of each porous ceramic.

Based on these results and SEM observations it was concluded that each porous ceramic consisted of a highly interconnected partly open-cell porous structure. This is essential to drug loading and drug release, as interconnected open pores are necessary to allow the flow of substances (Liu, 1997).

3.6. Drug loading of porous ceramic microparticles

The diltiazem HCl loading of N-light N3 achieved using loading method (i), which did not use a vacuum, was $5.47 \pm 0.80\%$ w/v. Method (ii), which applied a vacuum in the presence of drug solution, gave a loading of $6.25 \pm 0.44\%$ w/v. This method has most frequently been adopted in drug loading porous ceramics. There was no significant difference in the drug loadings obtained using methods (i) and (ii). However method (iii), which is a modification of method (ii) gave a significantly higher drug loading of $10.39 \pm 0.28\%$ w/v. Method (iii) proved more effective as it allowed displacement of the air within the pores of the ceramic with drug solution. During method (ii) the N-light N3 microparticles floated on the drug solution surface and therefore, although air was removed from the microparticles by applying a vacuum, it was not replaced with drug solution once atmospheric pressure was restored. If air were replaced by drug solution the particles would sink in the loading solution, as N-light N3 has a higher skeletal density than the loading solution. This only occurred using loading method (iii), which is further evidence that this method was the most effective loading technique. Based on these results this method was adopted for all subsequent loadings.

Table 2 shows the results of drug loading the porous ceramic microparticles using method (iii). Loadings of up to $12.67 \pm 0.62\%$ w/v were achieved, indicating the suitability of porous ceramic microparticles for delivery of both low

Table 2
Actual and theoretical drug loading of porous ceramics

Porous ceramic	Actual drug loading		Theoretical drug loading	
	Average (% w/v)	S.D.	Average (% w/v)	S.D.
N-light N3–Benzoic acid	8.72	0.40	14.51	0.11
N-light N3–Sodium benzoate	11.08	1.12	19.35	0.14
N-light N3–Diltiazem HCl	10.39	0.28	19.35	0.14
Starlight SLK1000–Diltiazem HCl	12.67	0.62	31.31	0.68
Carbolite 16/20–Diltiazem HCl	7.33	0.17	4.26	0.01

and high potency drugs and other chemicals. Factors that influenced drug loading were the concentration of the loading solution and the open porosity of the microparticles. No correlation between drug loading and surface area was seen.

The efficiency of loading was dependant on the bulk density of the porous ceramic, with Carbolite 16/20 loading most efficiently. The loading obtained was greater than the theoretical loading. This was possible as drug was deposited on the microparticle surface as well as in the pores during the loading process. The theoretical loading assumes drug loading only occurs within the pores. The reason Carbolite 16/20 loaded most efficiently was that during loading the microparticles remained beneath the surface of the loading solution at all times. However, with N-light N3 and Starlight SLK1000, the microparticles floated on the surface of the loading solution until the solution entered the microparticle pores. This made it possible for any air that had entered the sample tube to enter the microparticles in place of the desired loading solution.

3.7. Dissolution testing of drug loaded porous ceramic microparticles

Fig. 8 shows that N-light N3 gave sustained release for benzoic acid, sodium benzoate and diltiazem HCl, when compared to the dissolution profiles of the drugs alone. This was confirmed by calculating similarity factors (f_2) as listed in Table 3. In each case the value of f_2 was less than 50, whereas an f_2 value between 50 and 100 suggests that the compared dissolution profiles are similar

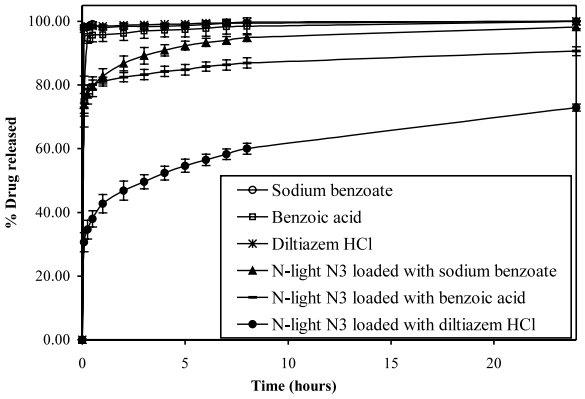

Fig. 8. Dissolution profiles of three drugs alone and when loaded into N-light N3 microparticles in phosphate buffer pH 6.8 at 37 °C.

(Tang and Gan, 1998). With only 72.92 ± 1.12% of diltiazem HCl released after 24 h, this release is the lowest of the three drugs. Diltiazem HCl also showed the lowest burst release of the three drugs. This was due to probable binding of cationic diltiazem HCl to the polyanionic surface of the microparticles.

Similarity factors showed the dissolution profiles of drug alone and those of crushed drug loaded samples of N-light N3 were similar (Table 3). This demonstrated the importance of the porous structure in providing sustained drug release. SEM confirmed drug was present within the microparticle pores. However, it was also observed on the microparticle surface (Fig. 9). Based on these results the burst release seen in the dissolution profiles was attributed to the presence of drug on the surface of the microparticle, while

Table 3
Similarity factors (f_2) comparing the dissolution profiles of drug alone versus those of the samples listed

Sample	Similarity factor	Sample	Similarity factor
Benzoic acid loaded N-light N3	42.7	Crushed benzoic acid loaded N-light N3	60.0
Sodium benzoate loaded N-light N3	40.9	Crushed sodium benzoate loaded N-light N3	85.2
Diltiazem HCl loaded N-light N3	13.1	Crushed diltiazem HCl loaded N-light N3	82.3
Diltiazem HCl loaded Starlight SLK1000	41.8		
Diltiazem HCl loaded Carbolite 16/20	21.1		

the sustained release was attributed principally to the location of drug within the pores.

Fig. 10 shows dissolution profiles of diltiazem HCl from each of the commercial porous ceramics. It can be seen that the choice of commercial porous ceramic is critically important in determining the release profile. The burst release for each porous ceramic was significantly different. The greatest burst release was from Starlight SLK1000 followed by Carbolite 16/20 and then N-light N3. Starlight SLK1000 also showed relatively poor sustained release compared to the other porous ceramics. While Carbolite 16/20 and N-light N3 gave different burst releases, both showed similar release profiles when the burst release at 2.5 min was subtracted from the data. This was confirmed by an f_2 value of 89.3. Similar to N-light N3, both Starlight SLK1000 and Carbolite 16/20 were polyanionic at pH 6.8 and therefore diltiazem HCl binding should have contributed to the sustained release observed.

Based on these results the ability of a porous ceramic to provide sustained release of a drug can be related to its pore size distribution. Starlight SLK1000 had large surface pores compared to N-light N3 and Carbolite 16/20 and therefore gave relatively poor sustained release. While it can be seen from Fig. 4(d) that N-light N3 has interior

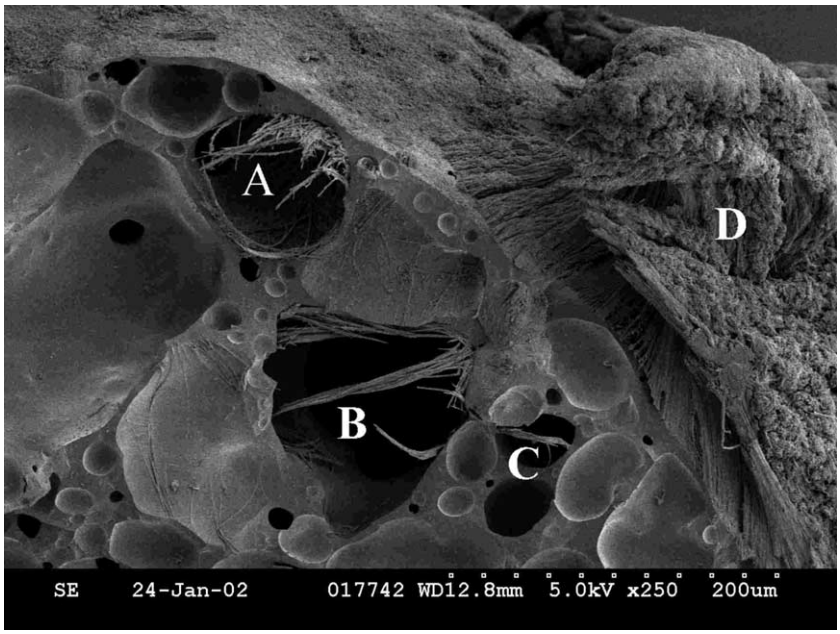

Fig. 9. SEM micrograph of sodium benzoate loaded N-light N3 (magnification ×250). Denoted by atypical morphology, pores containing sodium benzoate are located at regions A–C while surface associated sodium benzoate is located at region D.

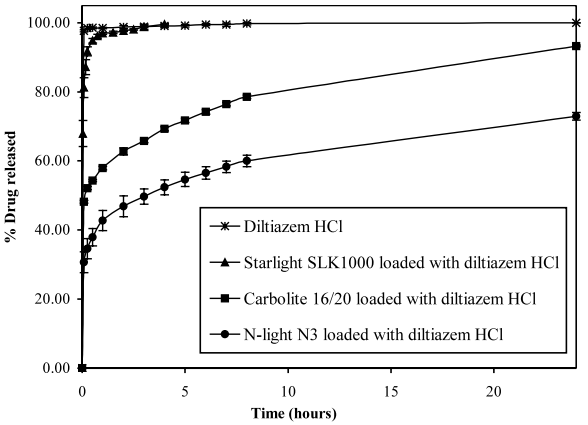

Fig. 10. Dissolution profiles of diltiazem HCl when loaded into Starlight SLK1000, Carbolite 16/20 and N-light N3 microparticles in phosphate buffer pH 6.8 at 37 °C.

pores of similar sizes to Starlight SLK1000, this did not result in poor sustained release as in order for drug to leave the porous ceramic it must exit through the smaller surface pores. The influence of pore size on drug delivery behaviour and the importance of porous walls with pores as fine as possible in order to provide lengthy sustained release has been noted by other authors (Krajewski et al., 2000; Netz et al., 2001).

4. Conclusions

Commercially produced porous ceramic microparticles with different porous microstructures can be drug loaded using a novel modification of the standard vacuum loading method. This method was designed to load floating porous ceramic microparticles and was significantly more effective than loading using the standard method. The drug loadings achieved indicate that porous ceramic microparticles would be suitable for the delivery of both low and high potency drugs. The loading was influenced by the drug solution concentration and the porosity and bulk density of the porous ceramic. Sustained release of drug from the porous ceramic microparticles occurred with the release influenced by the surface pore size distribution and by electrostatic interactions between both the interior and exterior microparticle surfaces and the drug. The presence of the porous microstructure was found to be essential in providing this sustained release.

The results indicate that porous ceramic microparticles should be suitable for the sustained delivery of drugs given orally. They are particularly suited for the delivery of highly water soluble cationic drugs, like diltiazem HCl. Release of such drugs should occur throughout the GIT, with the porous ceramic material remaining unabsorbed. This is expected, as similar materials, such as the aluminosilicates kaolin and bentonite, are not absorbed from the GIT. In the short term it is envisaged that porous ceramic microparticles will also be used for sustained chemical delivery. Examples of potential uses are in the controlled delivery of agrochemicals in pest control, reactants in chemical reactions or nutrients in biological media. In both sustained drug and chemical delivery, the release could be further modified by using mixtures of porous ceramic microparticles with a variety of properties. Another approach would be to load the microparticles with release modifying agents (lipids or polymers) or to coat the microparticles with a suitable film.

Future work will include the investigation of the aforementioned methods for modifying release. Secondly, aluminosilicate microparticulate porous ceramics with a range of properties will be produced from kaolin and halloysite. It is envisaged that porous ceramics based on halloysite will provide superior sustained release to existing porous ceramics, as the microtubular structure of halloysite can itself provide further sustained drug release.

Acknowledgements

This work was supported by an Enterprise Ireland Research Scholarship. The authors would like to thank the staff of the Centre for Microscopy and Analysis, Trinity College, Dublin for their advice and assistance in matters relating to electron microscopy. The authors would also like to thank Bioglan (Generics), Carboceramics, Imerys and Itochu Ceratech Corporation for donating materials.

References

Bechgaard, H., Ladefoged, K., 1978. Distribution of pellets in the gastrointestinal tract. The influence of transit time exerted by the density or diameter of pellets. J. Pharm. Pharmacol. 30, 690–692.

Ishizaki, K., Komarneni, S., Nanko, M., 1998. Porous Materials: Process Technology and Applications. Kluwer Academic, London.

Itokazu, M., Yang, W., Aoki, T., Ohara, A., Kato, N., 1998. Synthesis of antibiotic-loaded hydroxyapatite blocks by vacuum method and in vitro drug release testing. Biomaterials 19, 817–819.

Itokazu, M., Esaki, M., Yamamoto, K., Tanemori, T., Kasai, T., 1999. Local drug delivery system using ceramics: vacuum method for impregnating a chemotherapeutic agent into a porous hydroxyapatite block. J. Mater. Sci.—Mater. Med. 10, 249–252.

Kawashima, Y., Niwa, T., Takeuchi, H., Hino, T., Ito, Y., 1991. Preparation of multiple unit hollow microspheres (microballoons) with acrylic resin containing tranilast and their drug release characteristics (in vitro) and floating behaviour (in vivo). J. Controlled Release 16, 279–280.

Krajewski, A., Ravaglioli, A., Roncari, E., Pinasco, P., 2000. Porous ceramic bodies for drug delivery. J. Mater. Sci.—Mater. Med. 12, 763–771.

Landi, E., Orlandi, L., Spagna, G., Tampieri, A., Zaffaroni, N., 2000. Calcium phosphate ceramics as drug-delivery system for anticancer therapy. Key Eng. Mat. 192, 901–904.

Liu, D.M., 1997. Influence of porous microarchitecture on the in-vitro dissolution and biological behaviour of porous calcium phosphate ceramics. Mat. Sci. Forum 250, 183–208.

Montanaro, L., Jorand, Y., Fantozzi, G., Negro, A., 1998. Ceramic foams by powder processing. J. Eur. Ceram. Soc. 18, 1339–1350.

Moscou, L., Lub, S., 1981. Practical use of mercury porosimetry in the study of porous solids. Powder Technol. 29, 45–52.

Netz, D.J.A., Sepulveda, P., Pandolfelli, V.C., Spadaro, A.C.C., Alencastre, J.B., Bentley, M.V.L.B., Marchetti, J.M., 2001. Potential use of gelcasting hydroxyapatite porous ceramic as an implantable drug delivery system. Int. J. Pharm. 213, 117–125.

Queiroz, A.C., Santos, J.D., Monteiro, F.J., Gibson, I.R., Knowles, J.C., 2001. Adsorption and release studies of sodium ampicillin from hydroxyapatite and glass-reinforced hydroxyapatite composites. Biomaterials 22, 1393–1400.

Sepulveda, P., Binner, J.G.P., 1999. Processing of cellular ceramics by foaming and in situ polymerisation of organic monomers. J. Eur. Ceram. Soc. 19, 2059–2066.

Tang, Y., Gan, K., 1998. Statistical evaluation of in vitro dissolution of different brands of ciprofloxacin hydrochloride tablets and capsules. Drug Dev. Ind. Pharm. 24, 439–552.

Thoma, K., Alex, R., 1991. Biodegradable gentamicin-loaded controlled release implants made of beta-tricalcium phosphate ceramics. 2. Preparation and in vitro evaluation of gentamicin-loaded controlled release pellets. Pharmazie 46, 198–202.